AMDL

Auto-Rotation in Martian Descent and Landing

ESA Contract No. 21233/07/NL/CB

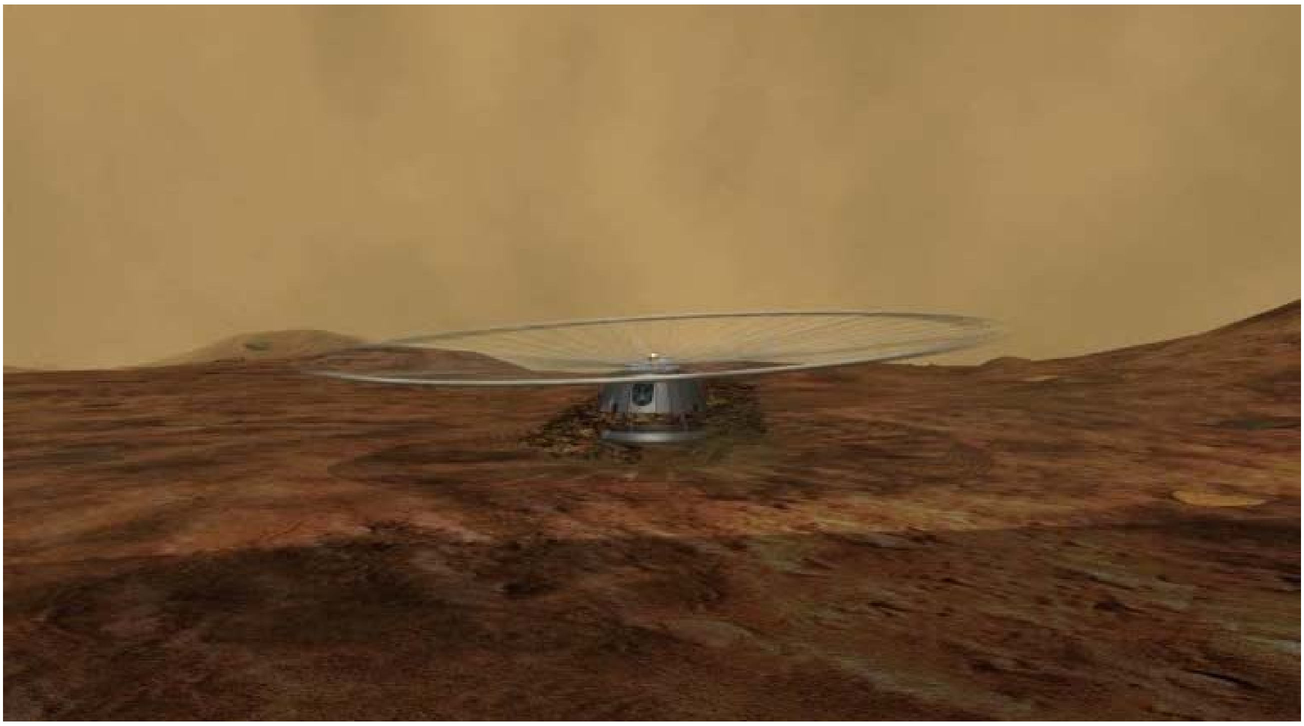

Executive Summary

Document D14: AMDL-RIBRE-TN-0014, Issue 1
Bremen, December 2009

Project Team

EADS Astrium, Bremen, Germany
Prime Contractor

Uwe Westerholt, Project Manager
Heinz-Günter Börchers, Thomas Elfers, Tobias Lutz, Peter Nöding,
Herbert Schmitke, Lüder Scharringhausen, Henning Schönbeck,
Susanne Waldewein

SRConsultancy, Stuhr, Germany
External Services

Stephen Ransom

Lindstrand Technologies Ltd
Sub-contractor

Dr. Per Lindstrand
Stacy Greensall, Steve Wallace

Windkanal Klotzsche, Dresden, Germany
Sub-contractor

Uwe Schönlebe, Dr. Wolfgang Schmidt, Gudrun Arnold

ESA Study Manager

Dr. Johan Köhler

1 Introduction

Within the next years several missions will take place to land scientific payloads on Mars. Most of the upcoming missions will deploy rovers, but also other scientific payloads are to be delivered to the surface. In the long term some missions aim at paving the way towards the first man-rated mission.

In this context one critical technology to master is the entry, descent and landing (EDL). While previous missions targeted to reach easy-to-access landing sites with minor precision requirements, the more ambitious scientific missions will have to cope with new issues. The main technology drivers in this context are the requirements to be able to land at higher altitudes, to perform precision landing and finally to perform hazard avoidance manoeuvres. The typical approach for such an EDL scenario is to use parachutes deployed at supersonic speeds in combination with powered soft-landing. Clearly, the performance of a powered lander is restricted by its amount of propellant, while all of its initial kinetic energy is dissipated during entry and parachute descent. This disadvantage might be avoided by the implementation of an auto-rotative descent and landing system.

Auto-rotation is a state of motion in which the air stream around a free-falling vehicle propels a rotor such that the rotor produces thrust. Helicopters use this principal to land safely in the event of turbine failure. With an auto-rotating vehicle it is possible to perform precision landing while maintaining complete controllability. A Martian EDL system based on auto-rotation can, therefore, decelerate after entry, like a parachute equipped system, and glide to a dedicated landing site reaching a down-range capability as high as 25 kilometres. The study performed for ESA describes such a system concept, its applicability and the need for technology demonstration.

The documentation supporting this study is to be found in References [1] to [18].

The work summarized here is based on the following requirements:

– the probe to be landed shall follow a ballistic entry trajectory,
– the probe shall have a Viking-like aeroshell,
– the probe shall be landed at altitudes below 2000 m,
– the probe shall be landed at a descent velocity of less than 20 m/s,
– the landing vehicle shall be capable of manoeuvring close to the surface prior to touchdown, and the landed mass shall be between 20 and 200 kg.

2 Mars, Entry, Descent and Landing Challenges

For scientific missions on Mars it is necessary to decelerate a probe from interplanetary arrival speeds of about 5 km/s to 7 km/s to nearly zero speed at touchdown. Typically most of the kinetic energy is dissipated during entry and to date most of the remaining kinetic and potential energy is dissipated during a parachute descent. A typical entry, descent and landing mission on Mars consists of the following phases:

- Entry
- Parachute deployment (at about Mach 1.5 - 2.0)
- Descent
- Retro-rocket braking (at about 100 m altitude and 60 m/s descent velocity)
- Airbag landing

Alternatively, powered landing missions (e.g. Viking) were performed in which the landing was achieved completely by thrusters and landing legs instead of retro-rockets and airbags. Reference [19] provides an overview of past and planned Mars exploration missions.

As the study is intended mainly to analyse the feasibility of an auto-rotation system for descent and landing on Mars, the focus has not been set on the entry phase. Nevertheless, the entry strongly influences the rotor deployment conditions, as it does also with the parachute deployment conditions in a "traditional" EDL scenario. It is also known that the ballistic coefficient of the entry vehicle significantly influences the rotor deployment conditions. The ballistic coefficient is defined as:

$$\beta = \frac{m}{C_D \cdot A_{ref}}$$

where: m = mass of entry vehicle,
C_D = drag coefficient, and
A_{ref} = aerodynamic reference area

For a Viking-like entry probe the drag coefficient around zero degree angle-of-attack (hypersonic ballistic entry) is $C_D \approx 1.6$. The reference area in this case is a circular area with a diameter d. For different entry vehicles the mass and the diameter are different thus leading to different ballistic coefficients.

As can be seen from Figure 1, the entry becomes steeper with increasing ballistic coefficient and the deceleration starts at lower altitudes. The result is a higher velocity at any given altitude (e.g. at 10 km the velocity for β = 50 kg/m² is 340 m/s and for β =

150 kg/m² it is 900 m/s). The blue zone in Figure 1 marks the zone of typical parachute deployment (dynamic pressures between 250 Pa to 1200 Pa and Mach numbers between 1.1 and 2.1). It can be seen that the entry flight paths with ballistic coefficients above 140 kg/m² do not pass through this region and hence cannot be used with ballistic entry missions. This limit will most probably decrease further when atmosphere variations are taken into account. Also, a ballistic coefficient of 30 kg/m² defines a lower limit.

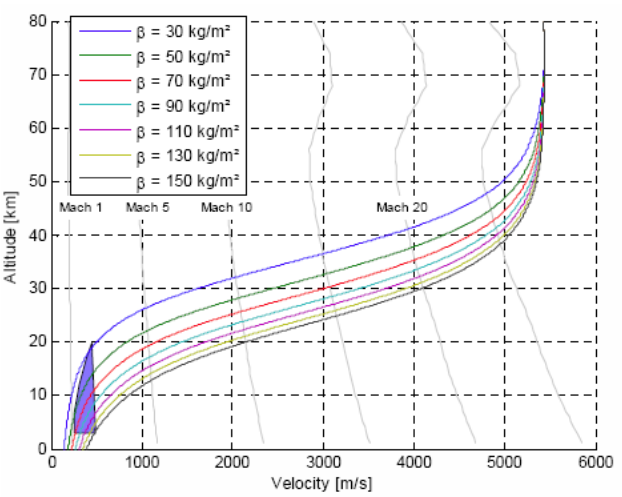

Figure 1: Flight path velocity - altitude diagram for entries with various ballistic coefficients

Probes are either controlled during entry in order to achieve lift at a specific angle-of-attack or enter on a ballistic trajectory. However, just before entry uncontrolled ballistic capsules are rotated with a small spin rate in order to provide spin-stabilization (Mars Pathfinder's roll-rate is 12 deg/s [20]). The design of the deceleration system has to take into account spinning motion which might tangle parachute lines or induce other undesirable effects.

Besides mission specific constraints arising from the entry, the selection of a target landing site is also of importance for EDL missions. Figure 2 shows the global topography of the surface of Mars as a function of surface elevation. While the northern hemisphere is well below the reference zero altitude, the southern hemisphere is mostly above. The southern hemisphere is on average six kilometres higher than the northern and contains older areological formations. Figure 3 depicts some of the past landed science missions as well as the envisaged landing altitude of the Mars Science Laboratory. From this figure it can be seen that most of the past missions reached landing sites in modest and easy-to-reach altitudes. Regions of interest are, nevertheless, located on the ancient highlands of the south. However, landing sites above 4 km altitude are relatively small parts of the whole planet. Landing missions should, therefore, aim for landing altitudes of up to 4 km. The altitudes were measured by the Mars Orbiter Laser Altimeter (MOLA). Future missions are, therefore, likely to aim for landings below this height.

Selection of a specific landing site depends on the goals of each individual mission and imposes constraints on the design of any landing system. An issue of importance is the hazard due to rocks in the landing area. The rock size and distribution defines the landing system as well as the desired method of landing (e.g. landing with a horizontal velocity component and a sled-like landing system).

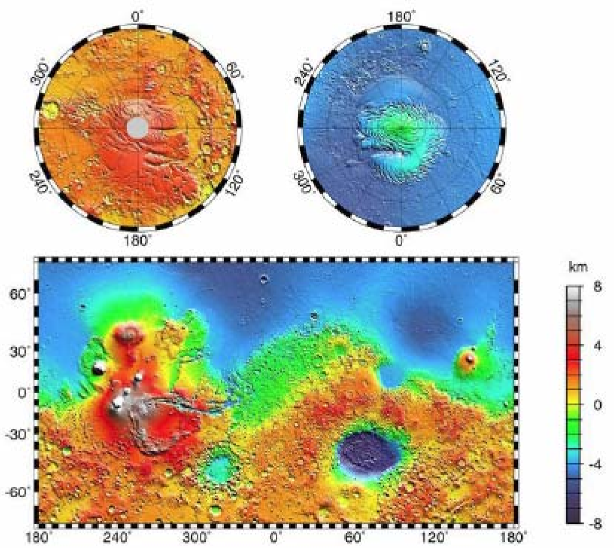

Figure 2: Maps of Mars global topography (Courtesy NASA/JPL-Caltech)

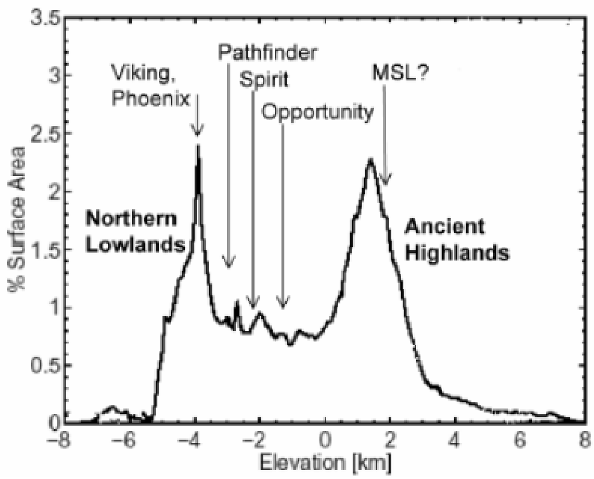

Figure 3: Mars elevation area distribution [20]

The above definition of the maximum target landing site altitude defines a lower limit for the deployment altitude. Assuming a parachute deceleration of typical missions, the vertical distance covered during deceleration is about 800 to 1000 m. Accounting for deployment delays due to sensor uncertainties and other sources, a loss of altitude of 1500 m should be assumed for the deceleration. Combining these with the desired landing altitude the deployment must be performed at least at an altitude above 5.5 km.

From Figure 1 it can be seen that for a parachute deployment at Mach 2.1, the minimum 5.5 km altitude can only be achieved by entry capsules with a ballistic coefficient less than 120 kg/m². The upper deployment altitude is not really limited despite the fact that higher altitudes at given Mach numbers are only reached for lower ballistic profile capsules. Therefore, the upper limit for a 30 kg/m² capsule would be 19 km. Such a capsule would very soon break through the upper dynamic pressure boundary and thus reach Mach 1.1 at a higher than allowed dynamic pressure. An upper limit of 19 km was, nevertheless, selected as the parameter range for further analysis. Table 1 summarizes the selected boundary conditions.

Parameter		Lower limit	Upper limit
Ballistic coefficient (entry)	[kg/m²]	30	120
Mach number	[-]	1.1	2.1
Dynamic pressure	[Pa]	250	1200
Deployment altitude	[km]	5.5	19

Table 1: Deployment conditions for parachute/auto-rotative EDL missions

In contrast to classical EDL missions, the mission sequence of an auto-rotation system is as follows:

– entry
– release of rotor cover
– deployment of rotor, establishment of auto-rotation state and deceleration
– release of heat shield (assuming traditional heat shield technology)
– glide phase
– flare
– touchdown

For a mission capable of meeting future requirements it will almost certainly be mandatory to provide full hazard avoidance capability and, therefore, the complete chain of EDL events should be designed to support guided flight operation. In order to ensure this type of operation, the orientation of the rotor disc of the deployed configuration must be fully controllable. Therefore, an auto-rotation based EDL system will have a high degree of autonomy and, when equipped with a dedicated sensor suite and a modern avionics system, it will have the following features:

- autonomous deployment of the rotor system as commanded by the guidance system
- guided flight to a dedicated target point
- autonomous performance of hazard avoidance manoeuvres (selection of new target point)
- flare manoeuvre to perform a soft and precise landing at the selected location

2.1 Transition from Entry to Descent

Transition from entry to descent takes place when the rotor is deployed. This is assumed to happen at Mach 2. Past missions tend to release the parachute at smaller Mach numbers but in order to reach landing sites at a high altitude an earlier deployment at higher Mach numbers is necessary. Rotor deployment is designed to take place at Mach 2 and at an altitude of approximately 10 km. The required target landing velocity is in the range from 10 m/s to 20 m/s. Figure 4 shows the velocity-altitude diagram for the transition to both landing velocities, the solid red lines indicating the velocity profiles for 10 m/s and 20 m/s landing speeds. It can be seen that after entry the capsule encounters the region of parachute/rotor deployment (blue zone). After deployment the velocity decreases until the vehicle achieves steady state descent. Depending on the target landing speed, the vehicle either decelerates faster at higher altitudes or slower at lower altitudes. The dotted line shows the entry trajectory to touchdown if no deceleration device is deployed. The final descent trajectories with 10 m/s and 20 m/s in this figure are assumed to be vertical.

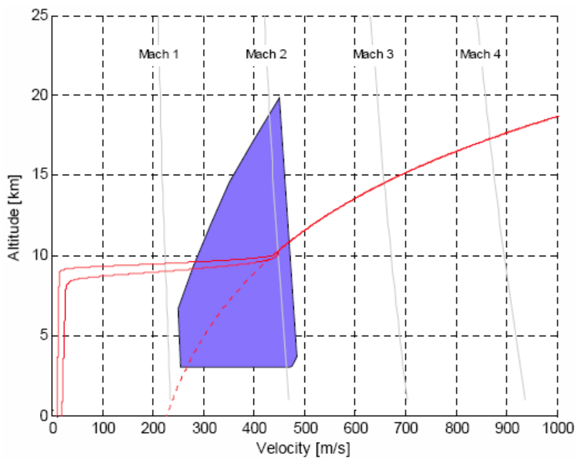

Figure 4: Altitude vs. Velocity for reference mission (β = 70 kg/m²)

It was found during first mission design iterations that it might be beneficial to use the lifting capabilities of the rotor even during deployment. However, at present it is not clear how this would interfere with the acquisition of auto-rotation and what the impacts will be on controllability. Therefore, it was assumed for the purposes of analysis, that during rotor deployment, the rotor disc will be perpendicular to the free stream and hence to the general motion of the vehicle. Glide and controlled flight will take place after the vehicle has been decelerated and a steady descent state has been achieved. During deceleration altitude is lost and, since it is an uncontrolled phase in terms of flight direction, down and cross range capability is also lost.

2.2 Glide Phase

During the glide phase it is possible to guide the auto-rotation system in a desired direction. Figure 5 shows the theoretically possible down range capability. For example, the lander could achieve a maximum down range of 28 km from an initial height of 8 km to reach a desired landing site at an elevation of 0 km assuming a lift/drag (L/D) ratio of 3.5.

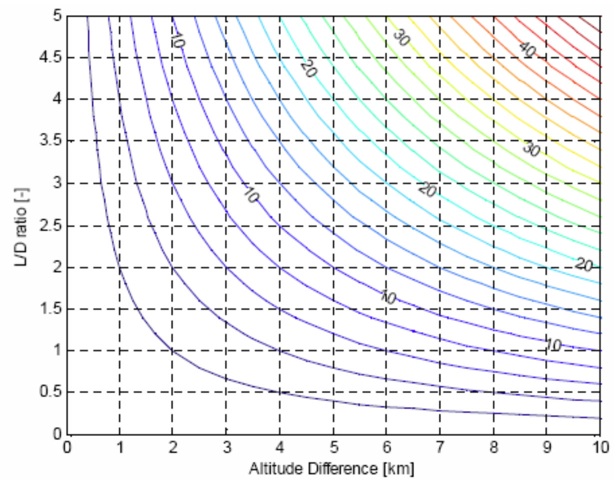

Figure 5: Down range (km) capability as a function of altitude difference and L/D ratio

However, two effects need to be considered. Firstly, if it is intended to land at higher altitudes, say 4 km, the possible achievable down range is reduced to 14 km. Secondly, if winds are encountered (which is most likely), then the down range capability might also be reduced since the wind alters the angle-of-attack and hence the L/D ratio. Furthermore, it might be necessary to perform a hazard avoidance manoeuvre, which, depending on the mission specific needs, imposes a minimum cross and down range requirement.

Figure 6 shows the down range capability of an auto-rotation system for a ballistic coefficient of 0.8 kg/m² and an 8 km altitude difference. It can be seen that, depending on the L/D ratio at lower wind velocities, flight against the wind is possible. When the wind increases, the down range capability is lost and even becomes negative. Changing the L/D ratio actively during flight by altering the angle-of-attack has a beneficial effect only on the down range if the drag is not increased.

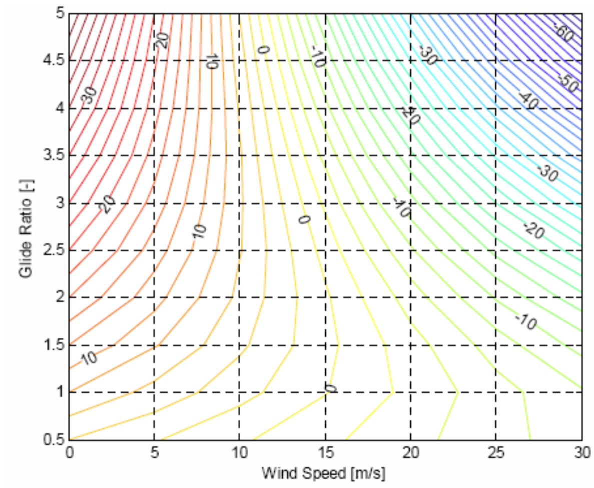

Figure 6: Down range (km) as a function of L/D ratio and wind speed (ΔH = 8 km, β = 0.8 kg/m²)

2.3 Flare and Touchdown

The gliding phase could include a flare manoeuvre prior to the actual landing. This manoeuvre can be performed in two ways:

- by pitching up the whole vehicle and thus reducing vertical speed while simultaneously decreasing lateral speed (maximum horizontal velocity component reduction will be achieved when pitching against the wind direction), or
- by increasing the collective pitch angle of the rotor blades.

In principal, the two options might also be combined and performed simultaneously.

3 Auto-rotation

The auto-rotation principle is based on the aerodynamic lift generated by freely-rotating (i.e. unpowered) rotor blades in forward and vertically-descending flight. Vehicles using this principle are termed autogyros. Unlike helicopter rotor systems, the autogyro rotor is mechanically simple and the blades do not necessarily require cyclic pitch control. Autogyros have been developed and flown with a moveable axis without cyclic pitch control or a fixed rotor axis with cyclic pitch control.

Auto-rotational landings of various types of vehicle have been conducted in terrestrial free flight trials and wind tunnels tests, and, practically, in emergency situations with helicopters since the

1920s. Interest in auto-rotation landing systems re-emerged in the 1950s and 1960s with schemes for the recovery of air-launched payloads, rocket boosters and manned lifting bodies and capsules as an alternative to parachutes and parafoils. In the event only parachutes were adopted for the retrieval of re-entry vehicles; rotor systems being considered difficult to develop, especially if deployed during the re-entry phase (aerothermodynamic technology development was required), mechanically too complex and difficult to install.

The most extensive investigation of auto-rotation landing systems was done by Kaman Aircraft Corporation in the period mid-1957 to mid-1967. At that time Kaman was interested in developing these systems for air-launched payloads but suggested that the system was applicable to the terrestrial recovery of space vehicles such as manned re-entry capsules [21]. Other proposals for auto-rotation EDL systems also considered inflatable rotors [22, 23].

Figure 7 shows the interaction of design parameters with the dynamic and kinematic parameters influencing the design of an auto-rotation EDL system.

A comparatively simple calculation to determine rotor sizes to meet the requirements specified in the Introduction can be based on estimates of the performance of a rotor system by applying momentum theory for an actuator disc model of a uniformly loaded rotor. The auto-rotation performance may be considered in terms of a drag coefficient based on rotor disc area and vertical descent velocity (leading to a drag coefficient $C_D \approx 1.1$).

Considering a vertical descent, the condition that the auto-rotation system drag should equal weight for the maximum permissible descent velocity at the elevation of the landing surface leads to the following simple formula:

$$d = \frac{1}{v} \cdot \sqrt{\frac{8 \cdot m \cdot g}{\pi \cdot C_D \cdot \rho}}$$

where: d = rotor diameter,
v = descent velocity,
m = landing mass including rotor system,
g = gravitational acceleration,
C_D = drag coefficient, and
P = atmospheric density

Therefore, the rotor diameter required is inversely proportional to the maximum permissible vertical speed at landing elevation and proportional to the square root of the total landed mass (landing mass and mass of descent and landing system).

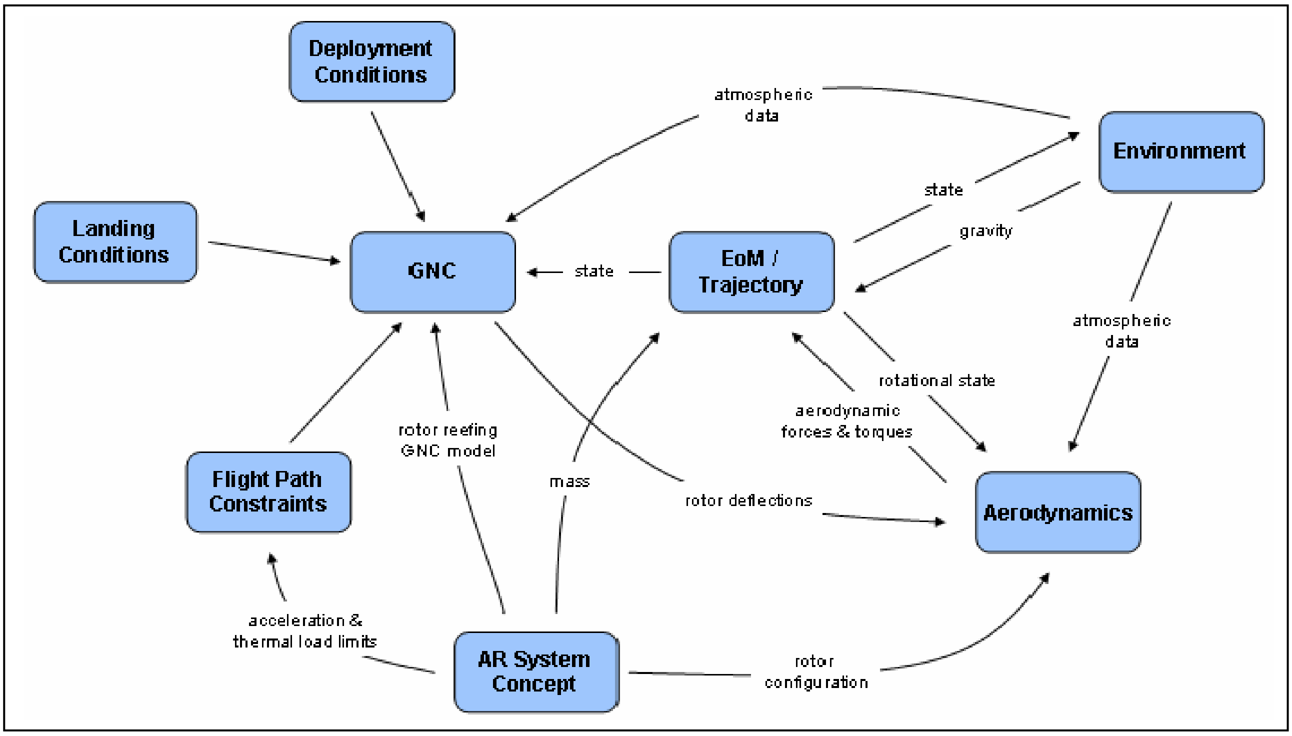

Figure 7: Design parameters and their interaction for an auto-rotation EDL system

The main considerations for initial rotor sizing can be summarized as follows:

- The rotor diameter is basically determined by the desired vertical descent velocity.
- The desired vertical descent velocity 10-20 m/s (ESA Specification) is high. However, glide operations with a forward speed component as well as landing flare allow significant reductions of sink rate compared to vertical descent.
- Blade geometry (chord length, aspect ratio) is determined by the number of blades and the desired rotor solidity.
- Maximum permissible rotor speed of rotation is determined by rotor blade tip Mach number limitation (Mach 0.8 - 0.9).

Assuming a single rotor system, a variation of key parameters reveals the dependencies shown in Figures 8 and 9, the former showing the required rotor diameter versus total landing mass for a vertical descent speed range of 10 to 20 m/s und Mars conditions at 0 m MOLA.

Figure 9 shows the non-linear increase of the rotor diameter with increasing EDL system mass. The shape of the curve allows the conclusion that the relative weight and size required for a rotor system-based EDL system tends to favour such applications towards heavier lander masses.

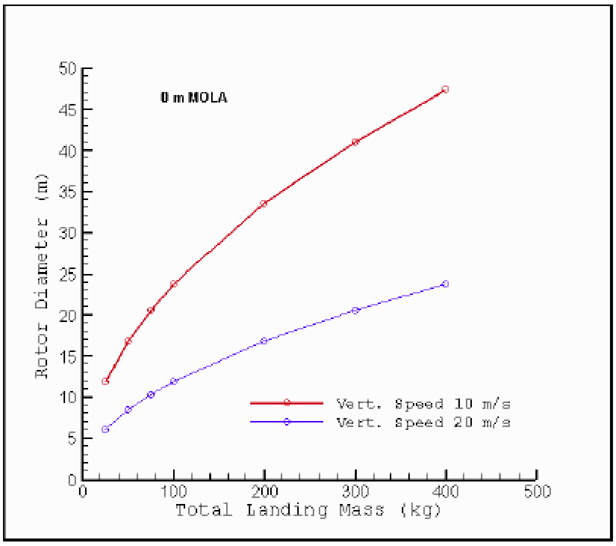

Figure 8: Required Rotor Diameter vs. Total Landing Mass (Mars conditions 0 m MOLA)

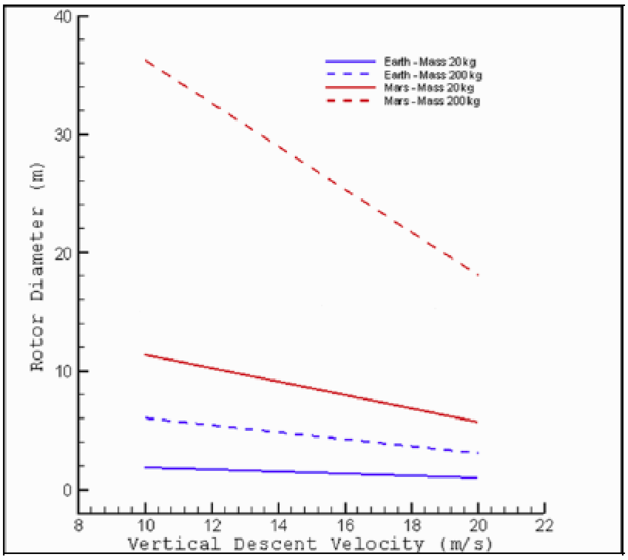

Figure 9: Comparison of Rotor Diameter vs. Vertical for a vertical descent speeds of 10 m/s and 20 m/s Descent Velocity for Mars and Earth (Mars conditions 0 m MOLA)

4 Inflatable Auto-rotation System Concept for EDL on Mars

Two basic rotor concepts were examined using data derived from Figures 8 and 9, namely, a “rigid” rotor system with telescopic blades (Figure 10) and a fully inflatable rotor system (Figure 11).

The potential advantage of the rigid rotor system might be seen in the fact that there exists a wealth of experience on the actual aerodynamic function of rotor systems made of rigid materials, at least for terrestrial applications. This also includes various rotor folding mechanisms to reduce hangar space required by larger helicopters. Of course, such folding mechanisms can in no way be considered fully comparable to the requirements for a rotor system to be unfolded in flight on Mars. Of relevance to telescopic rotor blade mechanisms, is the experience gained with of a high performance sailplane, the Akaflieg Stuttgart fs 29, which demonstrated the feasibility of varying the span of thin, high aspect ratio lifting surfaces by means of telescopic wings in flight. On the other hand, only limited actual experience exists regarding the aero-dynamic operation and performance of inflatable rotor systems.[24] However, inflatable fixed wing piloted and remotely-piloted aircraft have been demonstrated in actual flight under Earth conditions.

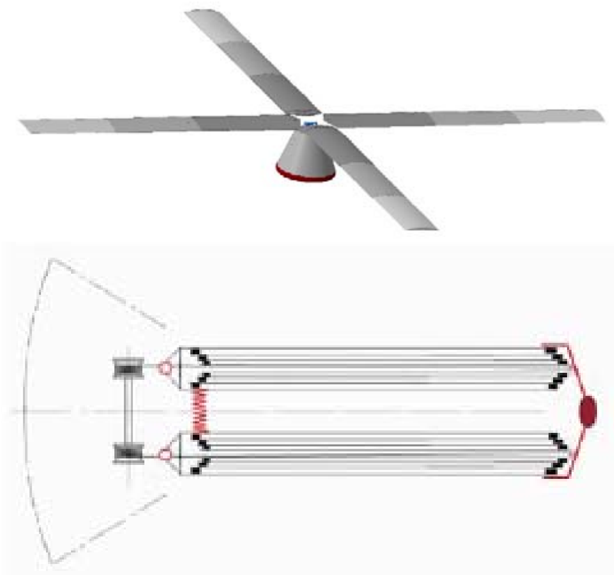

Figure 10: "Rigid" rotor system with telescopic blades

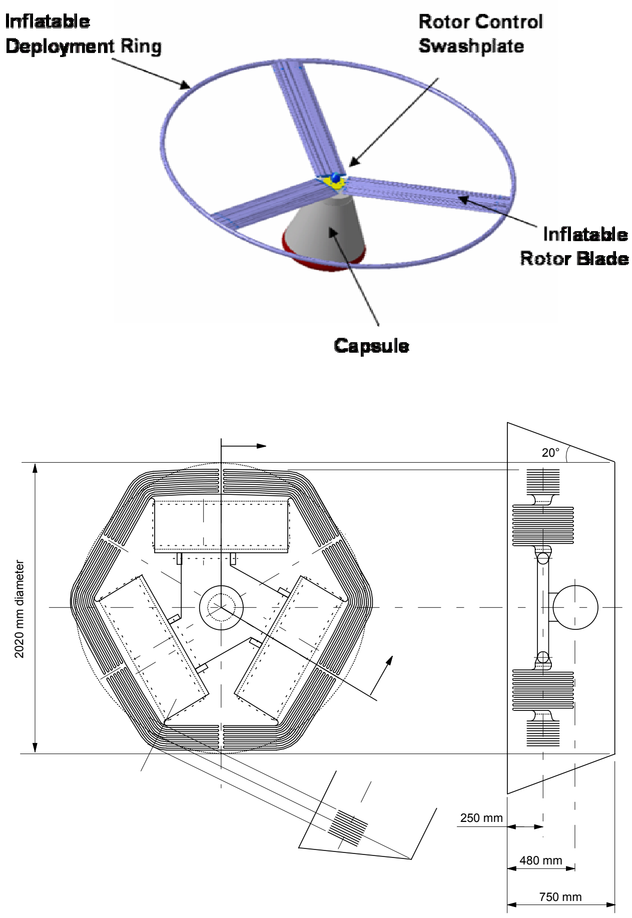

Figure 11: Inflatable rotor system concept

A detailed trade-off between these two basic options clearly favoured the inflatable system both in terms of mass and packaging. The rigid rotor system proved much heavier than the inflatable system and had a mass almost as much as the capsule it was intended to land. The three-bladed inflatable rotor mass/total landed mass fraction is of the order of 11% (descent speed 20 m/s, landed mass 200 kg, mean rotor diameter 19.30 m). The size of the stowed rigid rotors required them to be housed in a tail-like fairing behind the entry vehicle, whereas the deflated inflatable rotor was stowed in a flat circular compartment within the capsule's back shell. The inflatable rotor was selected as the more promising concept and a successful deployment test demonstration of the concept took place in the autumn of 2009.

The initial design of the inflatable rotor system concept was based on a rotor solidity factor of 0.08, a value defined for a vertical descent of 20 m/s at an altitude of 2000 m MOLA. This performance requirement allowed a three-bladed rotor system to be considered (Figure 11) but in order to achieve a sufficiently high gliding performance to allow lower touchdown speeds it was found necessary to increase rotor solidity to a value of 0.16. This situation led to a reconsideration of the method of packaging the deflated rotor without substantially increasing its stowage volume and resulted in a six-bladed rotor system. (Figure 12). The six-bladed inflatable rotor mass/total landed mass fraction is of the order of 18% (descent speed 20 m/s, landed mass 200 kg, mean rotor diameter 20.16 m).

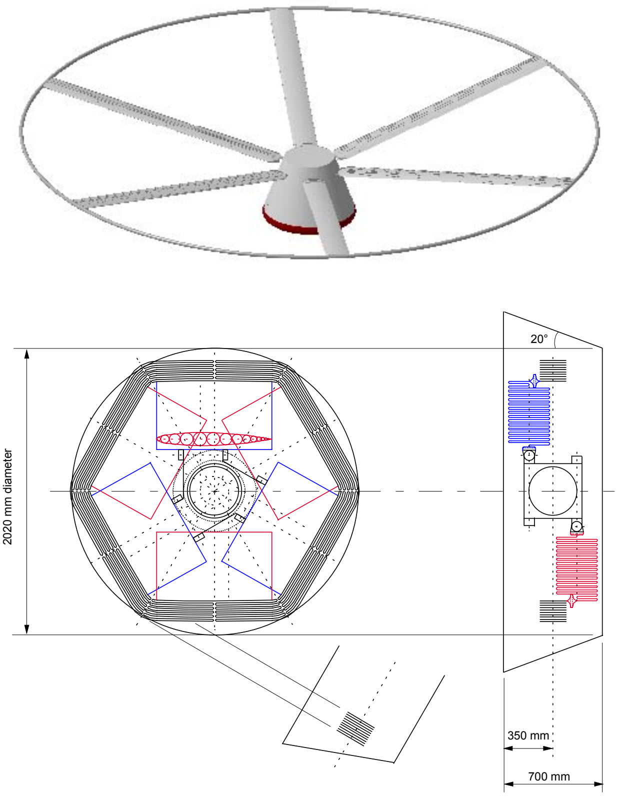

Figure 12: Improved inflatable rotor system concept

5 Simulation for System Evaluation

The logic for the system comparison is shown in Figure 13. Auto-rotation system concepts are defined by means of the integrated parametric design tool from specific requirements. The same requirements are applied to reference parachute based system concepts. Both system concepts are transferred to the ATPE simulator to simulate the trajectory and derive the landing state, which will enable a performance comparison to be made.

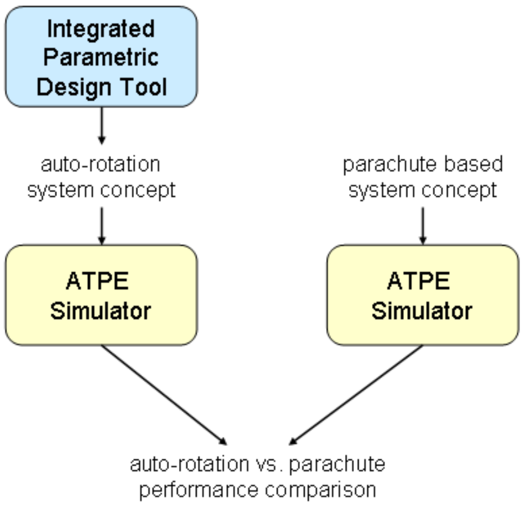

Figure 13: Simulation workflow and usage of tools

In order to produce comparable results, both lander system options must be based on the same requirements. The SOW requested consideration of landed masses between 20 and 200 kg and vertical landing velocities of 10 to 20 m/s. Table 1 identifies the options which were analysed in the study.

		Landed Mass [kg]		
		20	**100**	**200**
Landing Velocity [m/s]	**10**	Option 1	Option 3	Option 5
	20	Option 2	Option 4	Option 6

Table 1: System option designations

For all options, as defined in Table 1 and for the auto-rotation and parachute-based system concepts, the results were derived for:

- a landing site altitude of 0 m MOLA,
- a mean atmospheric density, and
- no and medium wind conditions

The entry conditions are the same for all options and both concepts and the initial and final conditions of the entry are given in Table 2.

All auto-rotation lander system options are derived using the integrated parametric design tool.[14]

All parachute-based lander system options are based on the Mars Pathfinder concept, in which a passive entry capsule deploys a disc-gap-band parachute. The vehicle descends under the parachute until retro-rockets are fired for terminal descent. A few metres above ground the vehicle's vertical velocity nulls-out and the lander is released from the backshell protected by airbags. The terminal descent thrust and the null-out altitude must be adapted individually to the specific option. The specific impulse of the retro-rocket system is assumed to be 250 s and the drag coefficient of the parachute is assumed to be 0.55.

Parameter		Value
Entry Conditions		
Flight Path Velocity	[m/s]	5800
Flight Path Angle	[deg]	-12
Entry Ballistic Coefficient	[kg/m²]	60
Deployment Conditions		
Altitude	[m]	10041.00
Flight Path Velocity	[m/s]	383.45
Flight Path Angle	[deg]	-28.40

Table 2: Initial and final conditions of the entry trajectory

5.1 Simulation Results Auto-Rotation System

The resulting landing velocities for all auto-rotation options are presented in Figure 14 (vertical landing) and Figure 15 (flare landing). For the vertical landing it can be seen, that options 1, 3 and 5 relate to the 10 m/s landing velocity requirement. Only the vertical component of the velocity is relevant in this analysis, since the lateral velocity induced by wind can be mitigated by the vehicle for the given wind profile. A positive effect of this mitigation is that the vertical landing velocity is slightly decreasing, when wind acts on the lander.

For the flare landing, only the horizontal component of the velocity is relevant since the tangential landing sequence reduces the vertical component to nearly zero. Flare landings reduce the landing velocity significantly. It is to be noted, that head and tail wind refers to the wind condition during the gliding flight. The landing is always performed against the wind direction.

The error ellipses and the mass factor of the auto-rotation options are presented inTable 3. It can be seen, that the error ellipses are smaller for the low landing velocity options. The mass factors are also smaller for the low landing velocity options.

5.2 Simulation Results Parachute-Based System

The resulting landing velocities for all parachute based options are presented in Figure 16 (vertical component) and Figure 17 (total velocity). It can be seen, that options 1, 3 and 5 relate to the 10 m/s landing velocity requirement. It can be noted, that the vertical velocity component increases only slightly when wind is acting on the vehicle. However, the total velocity increases strongly, since lateral velocity is induced.

All parachute-based options descend with the same descent speed profile. Therefore, their downrange error during descent is similar. The error induced by the parachute descent is roughly 1.8 km. The total error ellipse major axis of parachute missions is typically between 80 and 150 km. This includes errors arising from entry descent and landing.

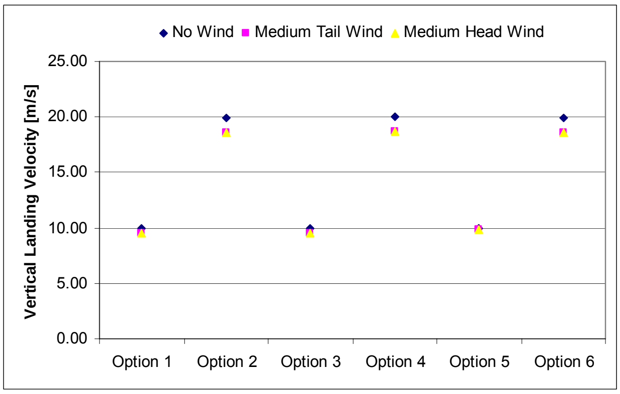

Figure 14: Vertical landing velocity of an auto-rotation configuration

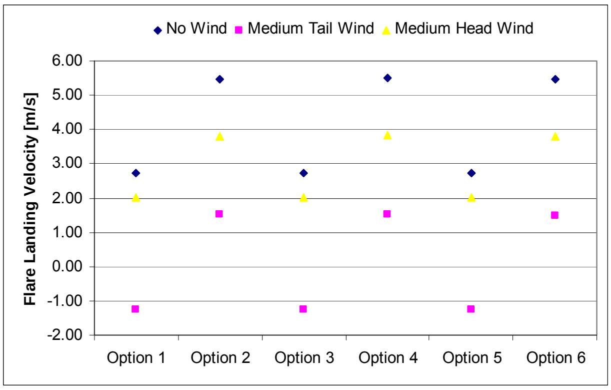

Figure 15: Flare landing velocity of an auto-rotation configuration

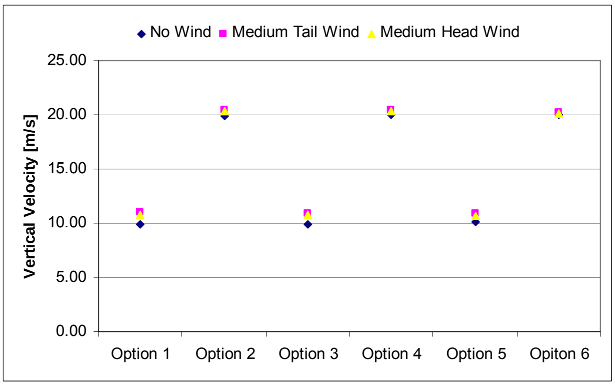

Figure 16: Vertical component of the landing velocity, parachute-based configuration

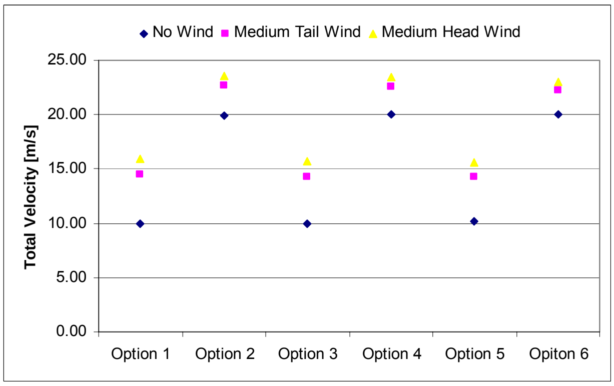

Figure 17:Total landing velocity, parachute-based configuration

	Option	1	2	3	4	5	6
Error ellipse major axis	Max [km]	121	135	121	135	120	137
	Min [km]	51	65	51	65	50	67
Landed Mass	[kg]	20	20	100	100	200	200
Entry Mass	[kg]	42	30	201	141	421	282
Mass factor	[-]	0.48	0.68	0.50	0.71	0.48	0.71

Table 3: Error ellipses and mass characteristics of auto-rotation configurations

5.3 Results from Simulation

The primary aim of the simulation was to establish a range of top-level mission parameters for which the inflatable auto-rotation system is potentially a viable or superior option. These parameters may include the figures of merit:

– fraction of payload mass with respect to entry mass
– maximum achievable landing site altitude
– landing accuracy in terms of error ellipse

However, other parameters, such as landing velocity, wind conditions, etc, can also be taken into account.

Noticeable from the results presented in Section 5.2 is that the landing velocity of the auto-rotation system can be significantly reduced when a flared landing is performed. This situation allows two design options:

1. a reduction in rotor dimensions which increases the flare landing velocity with the benefit of increasing payload mass as well, and
2. a tightening of the landing velocity requirement which might result in a simplified touchdown attenuation system (airbags, legs, sled, etc).

Therefore, the application of an auto-rotation system allows a soft landing in comparison to a parachute-based mission, which performs a semi-hard landing.

The simulation also revealed that the landing velocities of the auto-rotation system are less sensitive to wind effects. While for parachute-based systems the velocity increases, the auto-rotation system even benefits from moderate wind velocities. Since Mars is a windy place this helps to reduce mission uncertainties.

Another effect of applying the auto-rotation system is that it provides a significant glide capability which the parachute design does not have. This allows, at least, hazard avoidance manoeuvres and, in combination with guided entry, also precision landing.

The mass factors of the parachute systems were all assumed to be 0.62 for the analysis because of the estimation method. The mass factors of the auto-rotation system strongly depend on the vertical landing velocity and glide performance requirements. They vary between 0.48 and 0.71 within the analysis but even for the high velocity options (2,4 and 6), which have the highest mass factors, the flare landing velocity is below the landing velocities of the corresponding parachute-based options. Thus it seems to be very likely, that lighter systems can be achieved with an auto-rotation design resulting in an increased payload capacity.

When comparing the velocity results for different landing site altitudes it was found that the velocity stays constant for parachute-based systems. The reason for this is that the retro-rockets are fired to reduce the velocity to almost zero at a given altitude above the ground followed by a freefall of the lander. This is independent of the landing site altitude (LSA). In contrast, the velocities for an auto-rotation lander decrease with decreasing LSA because of the increasing atmospheric density. If the LSA is increased, then the landing velocity also increases. At this point the mission requirements need to be taken into account since increasing the LSA might result in harming landing velocity requirements.

LSA effects on downrange are different for the parachute-based and the auto-rotation systems. Downrange in terms of parachute systems basically relates to landing position error. The error ellipse increases with decreasing LSA. For the auto-rotation system there is a different perspective, since downrange relates to reducing the entry induced position error, i.e. lower LSAs increase the accuracy.

The highest achievable landing site is basically limited by the deployment altitude and velocity. The parachute or auto-rotation descent sequence is quite similar in terms of timing. The parachute is deployed and decelerates the lander which then descends until firing the retro-rockets 100 to 200 m above the ground. The rotor of the auto-rotation system is deployed and decelerates the lander which then descends until initiating the landing manoeuvre 100 to 200 m above the ground.

Top-level Mission Parameter	Auto-Rotation System	Parachute System
soft-Landing capability	+	–
wind effect mitigation	+	–
hazard avoidance	+	–
precision landing	+	–
payload mass capability	+	–
achievable LSA	–	+
heritage	–	+

Table 4: Top-level mission parameter evaluation

Table 4 provides an overview of some top-level mission parameters and shows which of the descent and landing system concepts better satisfies specific needs. From the discussion above it can be concluded, that the auto-rotation system offers soft precision landing capability with hazard avoidance and is capable of mitigating wind effects. Furthermore, a higher payload mass can be achieved with an auto-rotation system. Concerning the achievable landing site altitude, the major means of increasing it is to perform a guided entry. Thus both systems do not offer such a possibility. The main advantage of a parachute based system concept is its heritage.

5.4 Scaling effects

Scaling effects with respect to the size of the lander is understood as scaling the landed mass. With the scaling of the landed mass, all masses and dimensions, such as entry capsule diameter, entry mass, rotor storage volume and rotor diameter, are also scaled. These parameters are, furthermore, influenced by the selected rotor solidity. Figure 18 shows the influence of the landed mass on the rotor diameter at a constant landing site altitude. The representation includes a computation of the rotor system mass which is specific for the selected inflatable rotor system. It is not necessarily valid for different auto-rotation systems.

In Figure 18 the vertical landing velocity is shown as a function of the rotor diameter for different landed masses. Since the vertical landing velocity is usually a predefined requirement, the diameter of the rotor is scaled with the landed mass. An increase in the landed mass for a specific velocity (e.g. 15 m/s) leads to a higher rotor diameter (10 m → 24 m → 37 m). Decreasing the mass shifts the minimum achievable landing velocity towards lower values while also decreasing the required rotor diameter. However, the minimum of the specific mass line does not necessarily correspond to an optimal solution for the auto-rotation system. This situation is clarified from the following figures showing the relation between landing velocity, rotor diameter and rotor solidity (Figure 19) and the relation between Descent and Landing System (DLS) mass, rotor diameter and rotor solidity (Figure 20).

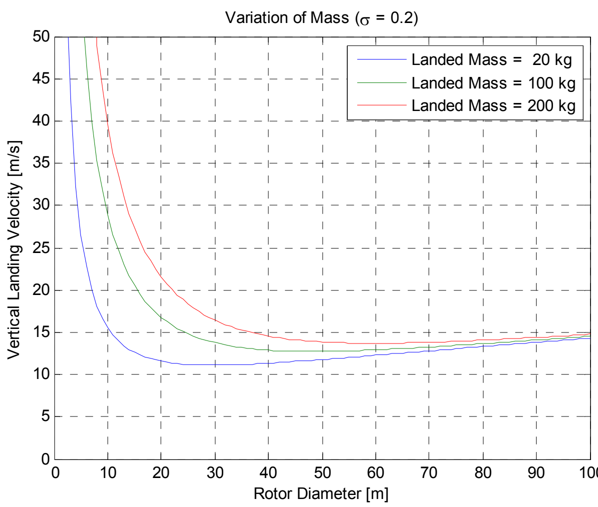

Figure 18: Velocity vs rotor diameter for different landed masses

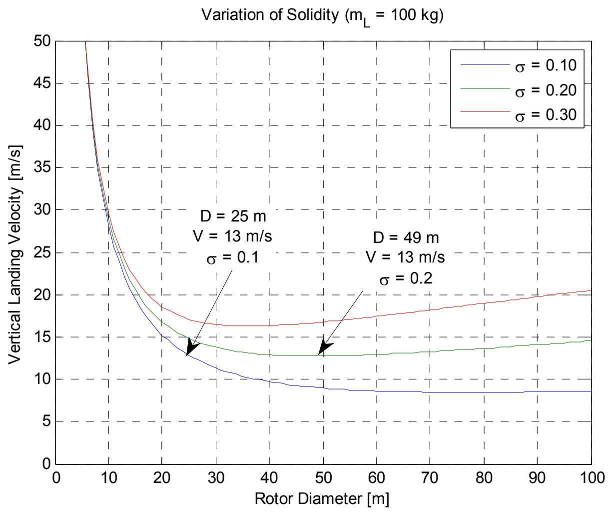

Figure 19: Velocity vs. rotor fiameter – variation in rotor solidity

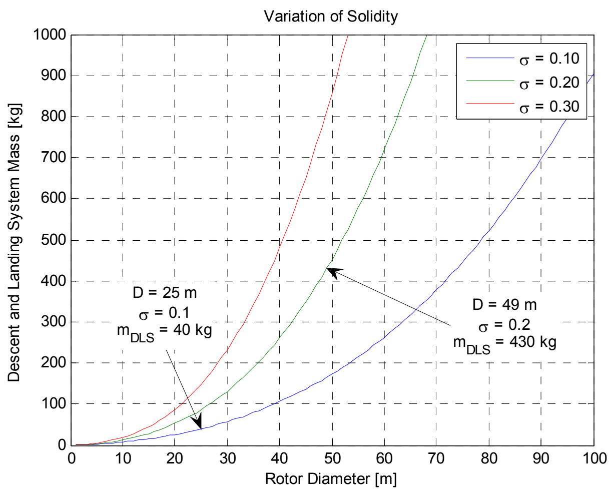

Figure 20: DLS Mass vs. rotor diameter – *variation in rotor solidity*

Obviously, there is a trade to be made between DLS mass and glide capability, since masses are limited by entry ballistic coefficients and launch vehicle capacity. The following points can be concluded from the analysis:

– for smaller landed masses and higher landing velocities the degree-of-freedom in the selection of rotor system characteristics increases, and
– high landed mass vehicles will need smaller solidities

6 Inflatable Rotor Demonstrator

The inflatable rotor demonstrator was designed and manufactured for terrestrial demonstration of its deployment in accordance with ESA's SOW.[1]

The general requirements for the design of a full-scale AMDL rotor are defined in Reference [3] and they were applied where appropriate to the design of the small-scale terrestrial demonstrator. It should be noted that the terrestrial demonstrator was required only to demonstrate successful deployment of the rotor blades by inflation but not necessarily a demonstration of transition to rotary movement after the deployment of the blades. In this case, design comprises were made with regard to the aero-dynamic profile of the rotor blade and the use of non-space-qualified materials, both aspects enabling a demonstrator to be designed and manufactured within the ESA-specified cost for the design, manufacture and testing of the demonstrator. Other features essential to the operation of the full-scale rotor were also not incorporated, e.g. pre-spin of the capsule on entry, swashplate control system and self-contained pressurization system.

Terrestrial demonstration took place in two phases, namely:

1. Development and testing of a single rotor blade which verified the overall strength of the blade material and material bonds. These tests were performed at different blade internal pressures and different materials with the object of determining the blade's strength and stiffness using different methods of fabrication, i.e. bonding or welding.[17,18] The blades were statically tested at up to an internal pressure of 500 kPa, the failure mode being delamination of the material at the bond or weld. The deploy-ment ring was statically tested at internal pressures up to 180 kPa.
2. Development and deployment testing of the inflatable rotor system:
   - at Lindstrand Technologies' premises: inflat-able part only,
   - at Astrium Bremen: complete rotor system acceptance tests, and
   - in the wind tunnel at Dresden-Klotzsche: complete rotor system installed in the lander.

The demonstrator was tested in the large, open-section, low-speed wind tunnel located at Dresden-Klotzsche with the plane of the rotor disc perpen-dicular to the airstream, i.e. the test simulated only the deployment phase and not the glide phase prior to touchdown of the lander. The diameter of the deployed rotor system (2.5 m) was defined by the size of the wind tunnel working section (3 m x 4 m).

The wind tunnel test conditions were determined from theoretical aerodynamic/aerothermodynamic analyses of the rotor/lander configuration using the well-proven DLR Navier-Stokes and Euler-Solver TAU Codes.

The freestream conditions which were selected roughly corresponded to a deployment altitude of 5300 m MOLA at Mach 1.75. At deployment, the flow is basically perpendicular to the rotor disc/rotor blades.

The corresponding freestream temperature and pressure under typical Mars atmospheric conditions were defined accordingly as T = 236.92 K and p = 436.18 Pa.

The CFD results for Mars conditions provided a basis for the definition of realistic loads to be applied under terrestrial wind tunnel test conditions to the reduced scale deployment demonstrator model of the inflatable rotor system. Figure 21 shows the pressure distribution (blue curves) along the centre-line of the rotor blade on the windward and leeward sides with the corresponding cut through the capsule and rotor blade outlined in black.

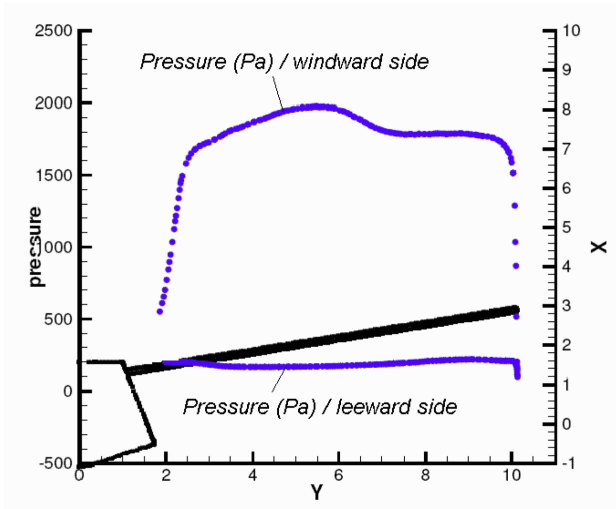

Figure 21: Pressure distribution along centre-line of the full-scale rotor blade

As can be seen from these results there is a pressure difference between front and rear side of the rotor blade of approximately 1800 Pa to 1900 Pa over most of the blade span, with the exception of a small area near the blade root where the flow is shaded by the capsule.

The absolute pressure levels are small even under supersonic flow conditions because of the compara-tively very thin Mars atmosphere. Therefore, deploy-ment seems feasible under these conditions, even if the inflating rotor blades attain their maximum radius initially outside the bow shock formed by the capsule heat shield at deployment Mach number.

It is worth mentioning that the flow conditions just after deployment indeed represent the dimensioning blade load case with its average blade loads at ~1850 N/m^2. In the following flight phases, during established auto-rotation operation, each of the six blades (single blade area ~ 8 m^2) of the reference design (244 kg total mass, meaning a weight force of 903 N for the design) on average has to support one sixth of the product weight x maximum manoeuvring load factor. If maximum load factors during auto-rotation manoeuvres up to n = 2 are allowed, this translates to comparatively quite low average blade loads below 40 N/m^2 during established auto-rotation.

The dominating aerodynamic similarity parameter identified for the deployment test under sea level atmospheric conditions on Earth are the dynamic pressure conditions approximating to the typical pressure loads on the blades, as obtained from the theoretical CFD analysis for Mars conditions.

In order to achieve a similar dynamic pressure in the same order of 1900 Pa in a wind tunnel with an open test section a freestream velocity of 55 m/s under Earth atmospheric conditions (density ~1.23 kg/m^3) is required.

The wind tunnel deployment tests were conducted with the three-bladed rotor system shown in Figure 11, which was redesigned to have a rotor solidity of 0.16. The inflatable parts of the rotor system were fabricated from Polyurethane-coated Rrip-stop Nylon. The fabric components were joined by welding: the aluminium rotor blade end ribs were bonded to the fabric. The blades were each made from a single piece of material with vertical spar webs, the flanges of the spars being RF-welded to the outer skin of the blade (Figure 22). The deployment ring was also made from a single piece of fabric. The ring was attached to the blades by a single hollow bolt reinforced with straps to prevent the rotor blades twisting relative to the plane of the ring during inflation. The air used for the inflation of the rotor was obtained from a ground source and distributed simultaneously through the rotor hub to each of the blades.

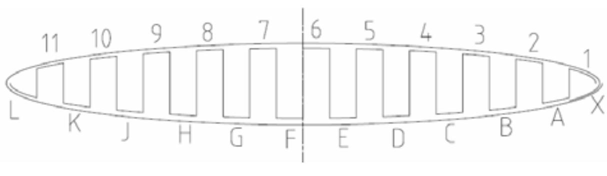

Figure 22: Cross-section of multi-web demonstrator rotor blade

The following inflation tests of the complete wind tunnel demonstrator model were conducted:

1. Acceptance/check tests were made at Astrium Bremen with the plane of the rotor disc suspended vertically. These tests were conducted at rotor internal inflation pressures up to 150 kPa to check for leaks and to obtain experience in packaging the deflated rotor.
2. An initial check of rotor deployment was conducted at zero wind speed in the wind tunnel (Figure 23). During this test a leak between one of the blade's outer skin and inboard end rib was found and repaired. An inflation test was afterwards performed to ensure that the repair had been made successfully. A rotor inflation pressure of 130 kPa was selected for this and all subsequent deployment tests.

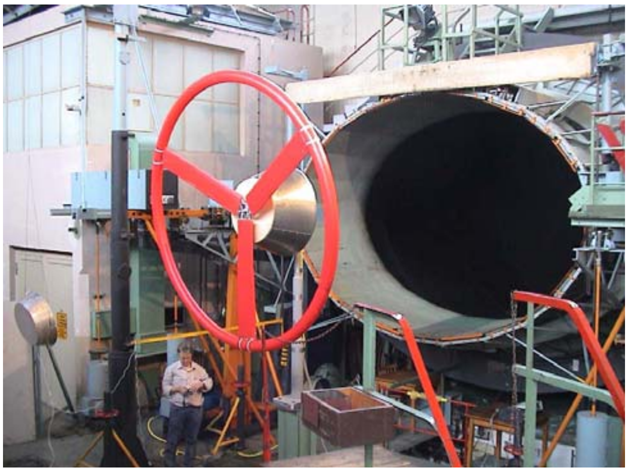

Figure 23: First deployment test at zero speed WKK Dresden, 18 August 2009

3. The first series of tests at speeds of 24.2 and 28.9 m/s were conducted with the capsule alone (rotor stowed and covered) Drag, lift, and side forces were measured.
4. The second series were conducted with the rotor pre-deployed at speeds between 11.7 and 15.1 m/s. These were made to assess the behaviour of the rotor with respect to vibration, flutter and distortion and to measure drag, lift and side forces of the deployed rotor system. The tests revealed a noticeable increase in blade dihedral due to drag.
5. **The third and final series of tests demonstrated successful deployment** (Deployment

sequence shown in Figures 24 and 25). The tests were conducted at speeds of 18.4, 20.4, 21.9 and 23.9 m/s. Full deployment was achieved in about 15 seconds during the first of this series of tests. Increases in speed up to 23.9 m/s resulted in greater deformation of the deployment ring primarily due to drag effects on the rotor .

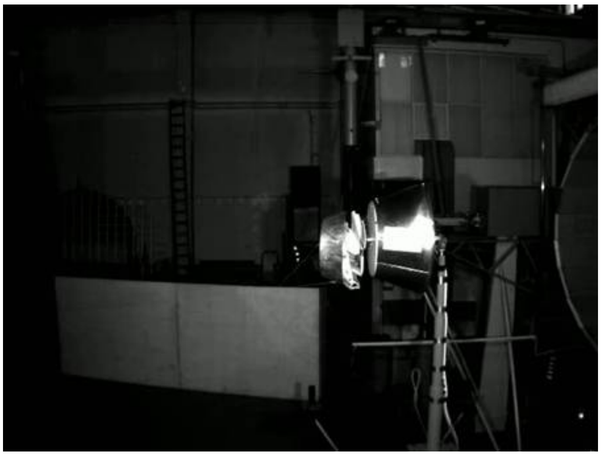

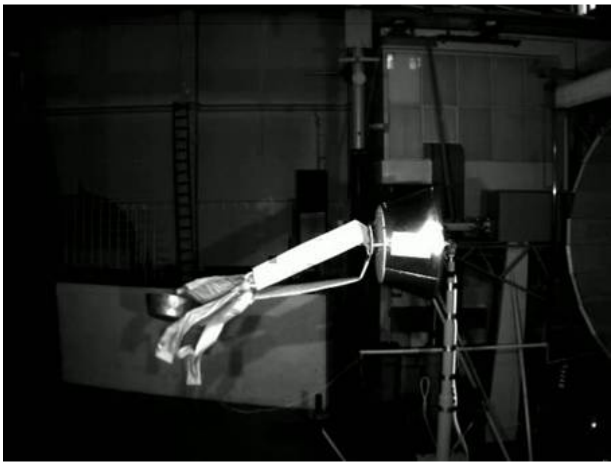

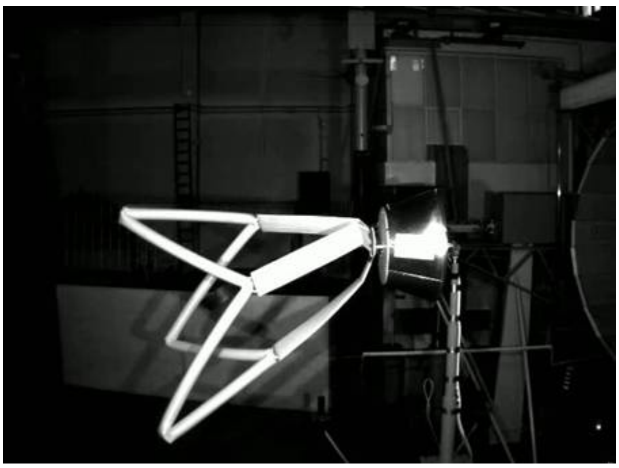

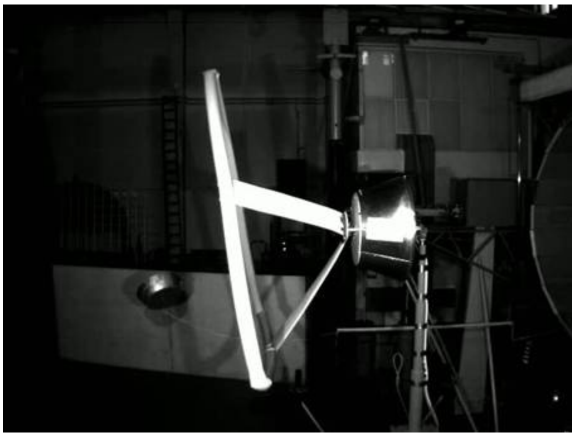

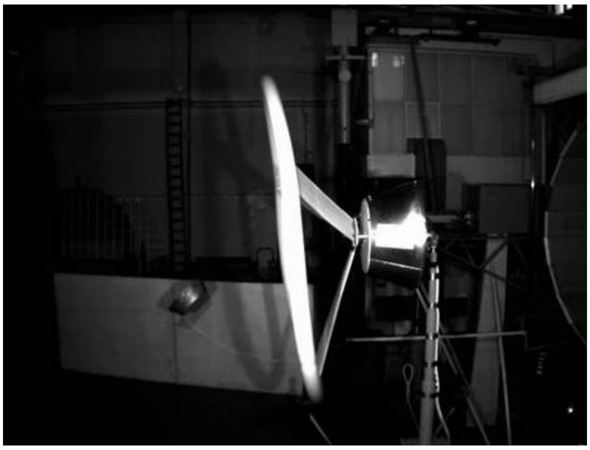

Figure 24: First of the successful deployment demonstration tests, V = 18.4 m/s, WKK Dresden, 19 August 2009

The tests verified the feasibility of deploying an inflatable rotor and the use of the ring in deploying the rotor from its downstream position immediately after release from the capsule to its operational position perpendicular to the airstream.

Leakage problems and pressure supply limitations did not allow a test at a wind speed of 55 m/s to be realized but the tests, nevertheless, achieved very satisfactory results up to 44% of the design aim.

The design of the inflatable rotor system demonstrator as tested will be considerably improved when inflated with a higher pressure. On going development on RF welding techniques by Lindstand Technologies have led to blade designs which can be inflated to 560 kPa.[18] These will be incorporated in the second demonstrator to be tested in 2010.

Improvements to the design inflatable rotor, based on lessons learnt during the deployment demonstration tests, are to be incorporated in the planned second demonstrator, which is planned to be tested in the spring of 2010.

Figure 25: Last of the deployment demonstration tests, V= 23.9 m/s WKK Dresden, 19 August 2009

7 Auto-rotation Applications to Venus and Titan Missions

Although the current study has focused on Mars applications, the use of the DLS rotor system has been assessed for missions to Venus and Saturn's moon, Titan.

Figure 26 shows the required rotor size vs. vertical descent velocity for different planetary bodies and a a range of landing mass of between 20 and 200 kg. Included are rotor sizes not only for Mars but also for Venus, Titan and Earth. As shown in this figure, the dimensions of the rotor systems for Mars have to be significantly larger than for equivalent requirements on Earth, requiring four to five times the rotor diameters.

However, it is clearly evident from Figure 26 and Table 5 how the dense atmospheres of both Venus and Titan are much more conducive to the application of rotor-based decelerators than the very thin atmosphere of Mars. Landers for Venus and Titan require rotor diameters more than an order of magnitude smaller (diameters of 1 m or less) for the desired landing mass range.

Nevertheless, it should not be overlooked that the environmental conditions on Venus are extremely challenging, such as surface temperatures in excess of 700 K, an atmosphere containing sulphuric acid and the very high atmospheric pressure of Venus. All of these conditions would preclude the use of an inflatable rotor system.

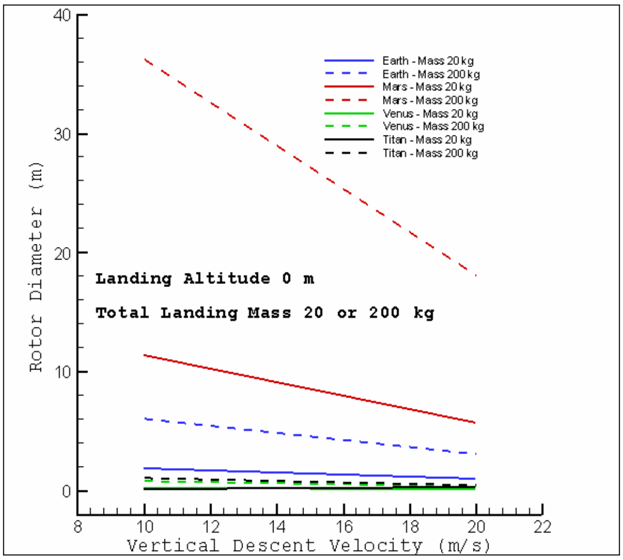

Figure 26: Rotor size vs. vertical descent velocity for different planetary bodies

Parameter	Earth	Mars	Venus	Titan
Density [kg/m³]	1.225	0.015	64.8	5.513
Pressure [KPa]	101.3	0.64	9200	147.9
Temperature [K]	288	214	720	94
Gravity [m/s²]	9.81	3.70	8.87	1.37
Speed of sound [m/s]	340	244	410	200

Table 5: Environmental conditions of planetary bodies

8 Conclusions

The present status of the study indicates that auto-rotation EDL systems are feasible within the limits specified by the requirements. Although the preferred concept relies on an "unconventional" approach, the study team considers that the risk associated with the development of an appropriate inflatable rotor system technology is acceptable and can be realized.

Compared with "rigid" rotor systems, the proposed inflatable concept offers a low installation mass. Auto-rotation EDL systems also offer the possibility of performing precision landings at relatively high elevations and low descent speeds when combined with a flared landing.

The deployment demonstrations of the inflatable rotor system verified the feasibility of the concept.

9 Acknowledgement

The authors sincerely thank ESA/ESTEC's project manager, Dr. Johan Köhler, for his support and the amicable discussions with him which took place throughout the study.

10 References

1. ESA, "Autorotation in Martian Descent and Landing", SOW, TECMMA/2007/209, Iss.1.0, 6 July 2007.
2. European Mars Climate Database: http://www-mars.lmd.jussieu.fr/mars/access.html
3. Astrium ST and SRC, "D1 – System Requirement Document for an EDLS based on Auto-rotation," AMDL-RIBRE-TN-0001, Iss.1, Bremen, 30 April 2008.
4. Astrium ST and SRC, "D2 – Auto-Rotation Performance Specification and System Concepts," AMDL-RIBRE-TN-0002, Iss.1, Rev.2, Bremen, 13 November 2009.
5. SRC, "D2 Appendix A – Auto-Rotation System Concepts and Trade-off," AMDL-SRC-TN-0002 A, Stuhr, 30 April 2008.
6. SRC, "D2 Appendix B – Mass Estimation of Inflatable Rotor System," AMDL-SRC-TN-0002 B, Iss.1, Rev.1, Stuhr, 9 October 2009.
7. Astrium ST and SRC, "D3 – Modelling Approach for the Performance Database Assembly," AMDL-RIBRE-TN-0003, Iss.1, Bremen, 30 April 2008.
8. Astrium ST and SRC, "D4 – Test Plan," AMDL-RIBRE-PL-0001, Iss.1, Bremen, 30 April 2008.
9. Astrium ST and SRC, "D5 – Development of a Performance Database in Atmospheric Entry, Descent and Landing," AMDL-RIBRE-TN-0005, Iss.1, Bremen, 5 February 2009.
10. Astrium ST, "D6 – Auto-Rotation Entry, Descent and Landing Performance Database," Software, Bremen, 2009.
11. Astrium ST and SRC, "D7 – Integrated Parametric Design Tool Development," AMDL-RIBRE-TN-0007, Iss.3, Bremen, 24 November 2009.
12. Astrium ST and SRC, "Integrated Parametric Design Tool – User Guide," AMDL-RIBRE-TN-0007 A, Iss.1, Bremen, 27 November 2009.
13. Astrium ST, SRC and LTL "D8 – Description of Demonstrator Design," AMDL-RIBRE-TN-0008, Iss.1, Rev.4, Bremen, 14 August 2009.

14. Astrium ST, “D9 – Integrated Parametric Design Tool,” Software, Bremen, 2009.
15. Astrium ST, “D10 & D11 – Auto-Rotation System Design and Evaluation,” AMDL-RIBRE-TN-0010, Iss.1, Bremen, 5 February 2009.
16. Astrium ST, SRC, LTL and WKK, “D12 – Rotor Deployment Proof-of-Concept Manufacture and Testing,” AMDL-RIBRE-TN-0012, Iss.1, Bremen, 2 December 2009.
17. LTL, “Beagle 3: Blade Candidate Comparison,” Technical Note RDTR-0327, Iss.1, Oswestry, 6 November 2009. (D12 Appendix A).
18. LTL, “Beagle 3: Phase 2 blade development record,” Technical Note RDTR-0325, Iss.1, Oswestry, 29 October 2009. (D12 Appendix B).
19. Braun, R. D. and Manning, R. M., “Mars Exploration Entry, Descent, and Landing Challenges,” *Journal of Spacecraft and Rockets*, Vol.44, No.2, 2007, pp.310-323. Available: http://emits.esa.int/emits-doc/ESTEC/AO-1-5422-RD2.pdf
20. Pathfinder website, accessed 4 July 2008: http://mars.jpl.nasa.gov/MPF/mpf/edl/edl1.html
21. Kaman Aircraft Corporation, “Investigation of stored energy rotors for recovery,” Technical Documentary Report ASD-TDR-63-745, Flight Dynamics Laboratory, Research and Technology Division, Air Force Systems Command, Wright-Patterson Air Force Base, Ohio, December 1963.
22. Levin, A.D. and Smith, R.C., “An analytical investigation of the aerodynamic and performance characteristics of an unpowered rotor entry vehicle,” NASA TN D-4537, April 1968.
23. Brunelle, E.J., Kershaw, T.N., Rayfield, W.P., and Sandor, G.N., “Landing on Mars by Autogyro,” *Rensselaer Review of Graduate Studies*, No.53, October 1968, pp.19-23.
24. Mansfield, D.L., “Preliminary Investigation of Ballute-Flexible Rotor Concept for Low Altitude Cargo Airdrop,” Final Report GER-12970, Goodyear Aerospace Corp, Akron, OH, August 1966.

11 Abbreviations

AMDL	Auto-Rotation in Mars Descent and Landing
ATPE	Aero-assist Technologies for Planetary Exploration
AUSM	Advanced Utility Simulation Model
CFD	Computer Fluid Dynamics
D	Document
DLR	Deutsches Zentrum für Luft- und Raumfahrt
DLS	Descent and Landing System
EADS	European Aeronautic Defence and Space
EDL	Entry, Descent and Landing
ESA	European Space Agency
GNC	Guidance, Navigation & Control
LSA	Landing Site Altitude
LTL	Lindstrand Technologies Ltd
MOLA	Mars Orbiter Laser Altimeter
NASA	National Aeronautics and Space Administration
PL	Plan
RF	Radio Frequency
SOW	Statement Of Work
SRC	SRConsultancy
ST	Space Transportation
TN	Technical Note
WKK	Windkanal Klotzsche